Available online at www.sciencedirect.com
ScienceDirect
Geochimica et Cosmochimica Acta 71 (2007) 4456–4473
Geochimica et Cosmochimica Acta
www.elsevier.com/locate/gca

Reductive transformation of iron and sulfur in schwertmannite-rich accumulations associated with acidified coastal lowlands

Edward D. Burton [a,*], Richard T. Bush [a], Leigh A. Sullivan [a], David R.G. Mitchell [b]

[a] Centre for Acid Sulfate Soil Research, School of Environmental Science and Management, Southern Cross University, Lismore, NSW 2480, Australia

[b] Australian Nuclear Science and Technology Organisation, Institute of Materials and Engineering Science, Menai, NSW 2234, Australia

Received 19 April 2007; accepted in revised form 6 July 2007; available online 26 July 2007

Abstract

We examined the transformations of Fe and S associated with schwertmannite ($Fe_8O_8(OH)_6SO_4$) reduction in acidified coastal lowlands. This was achieved by conducting a 91 day diffusive-flux column experiment, which involved waterlogging of natural schwertmannite- and organic-rich soil material. This experiment was complemented by short-term batch experiments utilizing synthetic schwertmannite. Waterlogging readily induced bacterial reduction of schwertmannite-derived Fe(III), producing abundant pore-water Fe^{II}, SO_4 and alkalinity. Production of alkalinity increased pH from pH 3.4 to pH ~6.5 within the initial 14 days, facilitating the precipitation of siderite ($FeCO_3$). Interactions between schwertmannite and Fe^{II} at pH ~6.5 were found, for the first time, to catalyse the transformation of schwertmannite to goethite (αFeOOH). Thermodynamic calculations indicate that this Fe^{II}-catalysed transformation shifted the biogeochemical regime from an initial dominance of Fe(III)-reduction to a subsequent co-occurrence of both Fe(III)- and SO_4-reduction. This lead firstly to the formation of elemental S via H_2S oxidation by goethite, and later also to formation of nanoparticulate mackinawite (FeS) via H_2S precipitation with Fe^{II}. Pyrite (FeS_2) was a quantitatively insignificant product of reductive Fe and S mineralization. This study provides important new insights into Fe and S geochemistry in settings where schwertmannite is subjected to reducing conditions.

1. INTRODUCTION

Schwertmannite ($Fe_8O_8(OH)_6SO_4$) is an Fe(III)-oxyhydroxysulfate that forms in acidic, Fe- and SO_4-rich waters (Bigham et al., 1990, 1996a,b; Murad and Rojik, 2003). As a consequence, schwertmannite is a common secondary mineral resulting from sulfide oxidation in rocks, soils and sediments (Bigham and Nordstrom, 2000; Bigham et al., 2002; Fanning et al., 2002; Blodau, 2006). It has been widely recognized in environments impacted by acid-mine drainage (AMD) (Bigham et al., 1996a; Murad and Rojik, 2003; Regenspurg et al., 2004; Acero et al., 2006). Schwertmannite has also been recently identified in iron-precipitate accumulations associated with acidified coastal lowlands (Sullivan and Bush, 2004; Burton et al., 2006a; Sullivan et al., 2006). Such landscapes are acidified as a result of drainage-induced oxidation of sulfides (mostly pyrite, FeS_2) in formerly waterlogged, sulfidic soils (i.e. acid sulfate soils; Fanning et al., 2002).

Schwertmannite is metastable and transforms under oxic conditions to goethite (αFeOOH). This transformation process has been found to proceed over timescales of several months to years. Bigham et al. (1996a) found that synthetic schwertmannite transformed to goethite over a period of 543 days, thereby lowering pH from 3.9 to 2.4 and releasing SO_4 and Fe to solution. Using natural schwertmannite, Acero et al. (2006) observed the formation of trace quantities of goethite within 105 days at pH 2–3. Recent studies

* Corresponding author.
E-mail address: ed.burton@scu.edu.au (E.D. Burton).

0016-7037/$ - see front matter © 2007 Elsevier Ltd. All rights reserved.
doi:10.1016/j.gca.2007.07.007

show that this transformation is accelerated at higher pH. For example, Jonsson et al. (2005) found complete transformation of natural schwertmannite to goethite within 187 days at pH 9, yet the transformation was incomplete after a period of 514 days at pH 6. Regenspurg et al. (2004) observed significant, yet incomplete, transformation of synthetic schwertmannite over 362 days at pH 7.

Several studies have examined the transformation of schwertmannite to goethite in oxidizing systems (Bigham et al., 1996a; Jonsson et al., 2005; Acero et al., 2006). However, schwertmannite transformations under reducing conditions have received little attention (Blodau, 2006). Under such conditions, schwertmannite-derived Fe(III) and SO_4 may be used as terminal electron acceptors by bacteria during degradation of organic matter (Blodau and Gatzek, 2006). The balance between Fe(III)- and SO_4-reduction is thought to control internal generation of alkalinity and acidity in schwertmannite-rich sediments (Blodau, 2006; Blodau and Knorr, 2006; Blodau and Gatzek, 2006; Knorr and Blodau, 2006). This, in turn, strongly influences water quality and the diagenetic Fe–S mineralization pathways (Peine et al., 2000; Burton et al., 2006b,c).

Studies of in-situ sediment profiles show that over time schwertmannite tends to be replaced by goethite and eventually by a suite of reduced Fe and S phases. Gagliano et al. (2004) observed replacement of schwertmannite by goethite with increasing depth in sediment profiles of an engineered AMD-treatment wetland. Peine et al. (2000) reported a relatively abrupt boundary between acidic schwertmannite-rich surface sediment and deeper goethite-rich, SO_4-reducing, subsurface sediments in an acid mine lake. Burton et al. (2006a) described similar behaviour in sediment profiles of waterways associated with acidified coastal lowlands, but also found accumulation of siderite ($FeCO_3$), Fe(II) monosulfides (FeS) and pyrite (FeS_2). These observational studies reveal much information regarding in-situ schwertmannite transformation products. However, the time-scales and geochemical controls on the relevant reductive mineralization pathways remain unclear and in need of further research (Blodau, 2006).

Sullivan and Bush (2004) demonstrated that schwertmannite accumulates in association with organic litter layers in acidified coastal lowlands of eastern Australia. The re-establishment of seasonal to semi-permanent wetlands in these degraded landscapes has been proposed as an environmental remediation approach (Tulau, 2002). However, the effect of this approach on reductive transformation pathways of Fe and S in schwertmannite-rich accumulations has not been examined. This is important as the rates and products of such transformations have profound implications for water quality and cycling of potentially toxic trace elements (Sullivan and Bush, 2004; Burton et al., 2006a,b; Sullivan et al., 2006). The lack of research into Fe–S behaviour associated with schwertmannite reduction also presents a significant limitation in understanding the fundamental geochemistry of acidified coastal lowlands.

In this contribution, we examine the reductive transformation of Fe and S in schwertmannite-rich soil material associated with acidified coastal lowlands. The objectives are to (1) identify the products formed from reductive transformation of schwertmannite, and (2) characterise the processes governing the formation and fate of the identified products. We conducted a long-term (91 days) diffusive-flux column experiment, designed to replicate waterlogging of natural schwertmannite-rich accumulations. This was complemented with short-term abiotic batch experiments involving synthetic schwertmannite. The results provide important new insights into Fe–S geochemistry in settings where schwertmannite is subjected to reducing conditions.

2. METHODS

2.1. General methods and reagents

All laboratory glass- and plastic-ware were cleaned by soaking in 5% (v/v) HNO_3 for at least 24 h, followed by repeated rinsing with deionised water. Reagents were analytical reagent grade (except where otherwise noted), and all reagent solutions were prepared with deionised water (milliQ). Deoxygenated solutions were prepared by purging with N_2 for at least 2 h (dissolved oxygen was routinely measured using a calibrated Orion Clarke-type electrode and meter and was consistently <0.01 mg/L). The mineralogy of all synthetic mineral phases was verified by X-ray diffraction (XRD). All solid-phase results are presented on a dry weight basis.

In the present study, total aqueous concentrations are presented without valence (e.g. Fe and SO_4), individual aqueous species are shown with a charge (e.g. $Fe(OH)^{2+}$ and CO_3^{2-}) and the sum of aqueous species for components with a specific redox state are indicated by superscripted Roman numerals (e.g Fe^{II} and S^{-II}). The sum of solid-phase species for components with a specific redox state are indicated by upper-case Roman numerals (e.g. Fe(III) and S(−II)).

2.2. Sample collection and manipulation

A sample of Fe(III)-rich ochreous material associated with the upper-most organic litter layer was collected from a *Casuarina*-dominated forest in eastern Australia (29°26′29″S, 153°14′12″E). The sample site was typical of low-lying (<2 m above sea-level) coastal landscapes, which experience acidification of surface-waters due to sulfide oxidation in acid–sulfate soils (Sullivan and Bush, 2004). Ochreous material, like that collected for the present study, is a common feature of acidified coastal lowlands. In these landscapes, schwertmannite typically occurs as coatings on organic leaf litter in low-lying areas prone to inundation by water (Sullivan and Bush, 2004). The sample described here was mainly comprised of very fine (~1 μm) spheroidal or rod-shaped aggregates of nanoparticulate schwertmannite encrusting *Casuarina glauca* leaf litter.

Within 24 h of collection, the sample was ground to <2 mm and homogenized. The collected sample was relatively dry (field moisture content = 6%) and it therefore was not possible to recover pore-water for characterization. Deionized water was added to the sample in order to achieve saturation (72% water w/w). The water saturated sample was stored at room temperature for 16 h (hereby

termed the initial sample) prior to commencement of the long-term column experiment.

2.3. Long-term column experiment

The long-term column experiment was designed to replicate freshwater inundation of schwertmannite-rich material in acidified coastal lowlands. In particular, the experiment simulated freshwater ponding—a land management strategy whereby artificially drained areas are essentially reverted back to freshwater wetlands (Tulau, 2002). The homogenized, saturated sample was added to a depth of 20 cm in a series of upright Perspex columns (length 30 cm, internal diameter 6 cm, sealed at bottom end). A 5 cm depth of surface water, comprising synthetic acid–sulfate water (ASW) was then added to the columns. The synthetic ASW was prepared as 1 mM KCl, 1 mM $CaCl_2$, 1 mM $MgCl_2$ and 15 mM Na_2SO_4 in 1 mM HCl. This composition was based on previous data for surface waters in acidified coastal lowlands (Burton et al., 2006a). The columns were incubated in the dark at 25 ± 1 °C using a thermostated water-bath. Twice weekly (Mondays and Fridays), 100 mL of surface water was retrieved using a pipette and replaced with fresh ASW.

Pore-water samples (5 mL) were retrieved from duplicate columns (prior to surface water replacement) at 3, 7, 14, 28, 49, 70 and 91 days post-inundation. This was achieved via sampling ports located at +1.5, −1.5, −4.5, −7.5, −10.5, −13.5 and −16.5 cm above (+) or below (−) the interface between the schwertmannite-rich material and the overlying surface water. Replicate columns were also sacrificed at 0, 7, 14, 28, 49, 70 and 91 days post-inundation for collection of solid-phase material. This involved removing the surface water, then incrementally extruding and collecting samples from the 0–3, 3–6, 6–9, 9–12, 12–15 and 15–18 cm depth intervals. Material from each depth interval was directly transferred into 50 mL polypropylene vials (this was completed in less than 1–2 min for each depth interval). The vials were completely filled with sample (no bubbles or headspace) and sealed with gas-tight screw-caps. Possible oxidation of reduced species was minimized by rapid sample retrieval and avoidance of unnecessary atmospheric exposure or sample disturbance. The solid-phase samples were stored frozen under N_2 until analysed.

2.4. Short-term batch experiments

The batch experiments were designed to examine potential short-term (24 h) interactions between schwertmannite and aqueous Fe^{II} (produced in the long-term column experiment via bacterial Fe(III) reduction). All experiments were performed under anoxic conditions in a glove-bag filled with high-purity N_2. The experiments were performed with analytical grade reagents, synthetic schwertmannite and thoroughly clean plastic- and glass-ware (i.e. acid-cleaned) and can therefore be assumed to reflect abiotic processes. The basic experimental approach involved (1) adding aqueous Fe^{II} (as various volumes of deoxygenated 1 M $FeSO_4$) to deoxygenated suspensions of synthetic schwertmannite (8 g L^{-1}), (2) adjustment of pH by drop-wise addition of deoxygenated 2 M NaOH and (3) allowing the system to equilibrate for 24 h. This necessary period for equilibration was based on research by Pedersen et al. (2005) into Fe^{II}-ferrihydrite interactions. Synthetic schwertmannite was prepared via H_2O_2 oxidation of a $FeSO_4$ solution (Regenspurg et al., 2004). The majority of experiments utilized a 0.05 M MES (2-morpholinopropanesulfonic acid)/0.05 M MOPS (2-morpholinoethanesulfonic acid) matrix as a pH buffer, with selected experiments using 0.05 M HCO_3 as a pH buffer.

2.5. Aqueous-phase properties

Surface- and pore-water samples were filtered to <0.45 μm using enclosed syringe-driven filter units (to minimize atmospheric exposure). Pore-water pH and redox potential were determined using probes calibrated against pH 4 and 7 buffers and Zoebel's solution, respectively. The pore-water pH was determined within a semi-enclosed sample cell designed to minimize $CO_{2(g)}$ degassing. Pore-water S^{-II} (which includes H_2S, HS^-, S^{-2} and aqueous sulfide complexes) was preserved with ZnOAc prior to determination by the methylene blue method (APHA, 1998). Aliquots of filtrate were added directly to 1,10-phenanthroline solutions for total aqueous Fe and Fe^{II} determination (APHA, 1998). Aqueous Fe^{III} was determined by the difference between total Fe and Fe^{II}. Alkalinity was determined by titration against 0.01 M HCl with the equivalence point determined using the Gran approach (Gieskes and Rogers, 1973). Calcium, K, Mg and Na were determined by inductively coupled plasma–atomic emission spectrometry (ICP-AES). Sulfate was determined by turbidimetric analysis (APHA, 1998). Chloride was determined by potentiometric titration (APHA, 1998). Dissolved Organic Carbon (DOC) was determined by the persulfate oxidation method (APHA, 1998). Activity coefficients for aqueous species were calculated by the Davies equation using MINTEQA2 (Allison et al., 1991; Allison and Purdue, 1994).

2.6. Solid-phase properties

Total C, N and S content was determined using an Elementar combustion analyzer. Total Fe concentrations were determined by aqua-regia digestion (1:3 HNO_3/HCl, 20 min, 1000 W microwave at 10% power) followed by ICP-AES analysis. Dithionite-extractable Fe was determined according to Rayment and Higginson (1992). The dithionite extraction procedure achieves quantitative recovery of Fe associated with goethite, schwertmannite, monosulfides and siderite. Reactive solid-phase Fe(II) and Fe(III) were recovered by anoxic extraction (20 h in the dark) with 0.2 M NH_4-oxalate/oxalic acid (adjusted to pH 3) (Phillips and Lovley, 1987) and analysed by the 1,10-phenanthroline method (APHA, 1998). When performed under anoxic conditions, the oxalate extraction procedure does not alter the oxidation state of the extracted Fe (Phillips and Lovley, 1987). The oxalate extraction quantitatively recovers all Fe(II) from Fe-monosulfides and siderite, as well Fe(III) from schwertmannite. The recovery of goethite (synthesized following Cornell and Schwertmann, 2003) during the oxa-

late extraction was examined in the presence and absence of 2 mM Fe^{II} (added as $FeSO_4 \cdot 7H_2O$ to the oxalate solution). Goethite recovery was minor (<3%) in the absence of Fe^{II}, yet substantial goethite recovery ($63 \pm 4\%$) was observed in the presence of Fe^{II} (due to the catalytic effect of Fe^{II} in enhancing oxalate-extractability of Fe(III)-oxyhydroxides; Kostka and Luther, 1994).

Solid-phase S fractionation was determined by sequentially extracting: (1) acid-volatile sulfide and acid-extractable SO_4, (2) elemental S and (3) pyrite–S (Burton et al., 2006a). Acid-volatile sulfide (AVS) was extracted by the diffusion method described by Hsieh et al. (2002) using a modified apparatus. Approximately 2 g of wet sample was equilibrated (orbital shaking at 150 rpm for 18 h) with 10 mL of 6 M HCl/0.1 M ascorbic acid in gas-tight 55 cm^3 polypropylene reactors. The evolved $H_2S_{(g)}$ was trapped in 7 mL of 3% Zn acetate in 2 M NaOH, and subsequently quantified via iodometric titration. The quantitative recovery of AVS was verified in the range 20–250 μmol with the use of standardized S^{-II} solutions (prepared from $Na_2S \cdot 9H_2O$) and freshly prepared suspensions of nanoparticulate mackinawite. The mackinawite was prepared directly within the AVS reactors by mixing equimolar quantities of Fe^{II} and S^{-II} (Wolthers et al., 2003). The recovery of AVS from both S^{-II} solutions and nanoparticulate mackinawite was $96 \pm 4\%$. Pyrite–S is not extracted by the AVS analytical method employed here (Hsieh et al., 2002). This was confirmed with the use of micro-crystalline pyrite that was synthesized following Schippers and Jorgensen (2001).

The slurry remaining after AVS extraction was diluted to 50 mL with deionised water and centrifuged (4000*g*, 10 min). An aliquot of the supernatant solution was removed for analysis of extracted SO_4 (hereby termed "acid-extractable SO_4") and the remaining solution discarded. As an aid in interpreting acid-extractable SO_4 data we examined extractability of schwertmannite and goethite. Schwertmannite and well-ordered goethite were synthesized as described above. Poorly-ordered goethite was also synthesized via a previously unidentified reaction between 40 mM Fe^{II} and synthetic schwertmannite at pH 6.5 (see Section 3). Schwertmannite completely dissolved during the acid extraction procedure (i.e. 18 h shaking in 10 mL of 6 M HCl/0.1 M ascorbic acid). In contrast, goethite recovery was variable, ranging from 100% for nascent poorly-ordered goethite formed from Fe^{II}-catalysed transformation of precursor schwertmannite to $64 \pm 8\%$ for well-ordered goethite.

Elemental S ($S^0_{(s)}$) was extracted by shaking the residual sample with 10 mL of chloroform for 16 h (Yao and Millero, 1996). An aliquot of the chloroform phase was analysed for S^0 using cold cyanolysis in acetone (Bartlett and Skoog, 1954). Residual $S^0_{(s)}$ was then removed from the sample by three rinses with 25 mL of acetone, and a final rinse with 20 mL ethanol. Each rinse involved 10 min of shaking, with the sediment and acetone/ethanol phases separated between rinses by centrifugation at 4000*g* for 10 min. This rinsing protocol was performed to minimize the quantity of $S^0_{(s)}$ that was carried over into the subsequent step (pyrite extraction) of the fractionation procedure. The residual AVS- and $S^0_{(s)}$-extracted sediment was then transferred into a 250 mL pyrex erlenmeyer flask. Pyrite–S was determined in the residual material by Cr(II)-reduction analysis as described by Sullivan et al. (2000).

Samples were dried at room temperature under a stream of high purity N_2 and examined by XRD and scanning electron microscopy (SEM). The dried samples were exposed to air for <2 min prior to commencement of XRD in order to minimize potential oxidation-induced changes in mineralogy. X-ray diffractograms were obtained for randomly oriented powders using a Phillips PW 1050/70 diffractometer with a Cu X-ray tube. Samples were step scanned from 10°2θ to 65°2θ using a 0.05°2θ step and a 3 s count time. Samples for SEM examination were mounted on aluminium stubs, coated with carbon, and the elemental composition and morphology of selected specimens determined using a Leica 440 SEM with an ISIS energy dispersive X-ray (EDX) microanalysis system. A quantitative peak-to-background EDX method for rough-surfaced specimens was used (Sullivan and Bush, 1997). Samples for transmission electron microscopy (TEM) were prepared following Ohfuji and Rickard (2006). The TEM observations were obtained with a JEOL JEM-2010F operated at 200 kV and fitted with a Gatan Imaging Filter. Selected area electron diffraction (SAED) patterns were collected using a 2.5 cm camera length.

3. RESULTS AND DISCUSSION

3.1. Properties of the initial schwertmannite-rich material

The initial sample was acidic (pH 3.4) and rich in organic C (Table 1). The pore-water had an Eh of 520 mV, which

Table 1
Selected properties of the initial schwertmannite-rich soil material examined in the present study

Solid-phase	
Organic C	$26.1 \pm 0.6\%$
Total	
N	$1.12 \pm 0.02\%$
S	478 ± 18 μmol g^{-1}
Fe	4105 ± 81 μmol g^{-1}
Dithionite-extract	
Fe	3697 ± 84 μmol g^{-1}
Oxalate-extract	
Fe(III)	3107 ± 66 μmol g^{-1}
Fe(II)	318 ± 33 μmol g^{-1}
Pore-water	
pH	3.4
Eh (SHE)	520 ± 25 mV
Fe^{II}	7.08 ± 0.2 mM
SO_4	31.1 ± 0.9 mM
Cl	428 ± 10 mM
Ca	14 ± 0.3 mM
K	6.8 ± 0.2 mM
Mg	47 ± 0.5 mM
Na	353 ± 25 mM

The reduced S species (AVS, $S^0_{(s)}$, and pyrite) were undetectable (<1 μmol g^{-1}). The pore-water Fe^{III} concentration was also undetectable (i.e. Total Fe differed from Fe^{III} by <3%).

indicates oxic conditions (Langmuir, 1997). The pore-water also contained relatively high concentrations of Fe and SO_4, with >97% of aqueous Fe being present as Fe^{II} (Table 1). X-ray diffractometry shows that the sample was mineralogically dominated by schwertmannite (Fig. 1). The schwertmannite was present as spheroids (~0.5 μm) or surface coatings with the typical "hedge-hog" morphology (Fig. 2) (Bigham et al., 1990; Regenspurg et al., 2004; Sullivan and Bush, 2004). The ratio of oxalate- to dithionite-extractable Fe was high (0.93), consistent with complete dissolution of schwertmannite during the oxalate-extraction procedure (Bigham et al., 1990; Dold, 2003). The sample contained abundant oxalate-extractable Fe (3425 μmol g^{-1}), of which 91% was the Fe(III) species. The observed oxalate-extractable Fe(III) concentration (3107 μmol g^{-1}) indicates that initial sample had a schwertmannite content of ~30% (w/w). The ratio of oxalate-extractable Fe(III) to acid-extractable SO_4 (after correcting for pore-water Fe and SO_4) was 6.9, which is comparable to a ratio of 8 for the ideal schwertmannite stoichiometry. This divergence from the ideal stoichiometry can be attributed to the presence of surface-adsorbed SO_4 (Bigham et al., 1990; Jonsson et al., 2005).

3.2. Long-term column experiment

Inundation (by freshwater ponding) induced Eh decreases from +520 mV to ~+100 mV and pH increases from pH 3.4 to pH ~6.5 within the initial 28 day period (Fig. 3). At these pH values, the Eh data indicate a shift from oxic to anoxic conditions. The development of anoxic conditions is attributable to bacterial metabolism involving partial degradation of organic material. The importance of this process is reflected in substantial increases in pore-water DOC during the early stages of the experiment (Fig. 3). Pore-water Fe^{II}, SO_4 and alkalinity also increased during the initial 14 day period (Fig. 3), which is consistent with the reductive dissolution of schwertmannite:

$$CH_3COOH + Fe_8O_8(OH)_6(SO_4)_{(s)} + 12H^+ \rightarrow 2HCO_3^- + 8Fe^{2+} + SO_4^{2-} + 10H_2O \quad (1)$$

Reduction of schwertmannite-derived Fe(III) occurs readily at low pH (Blodau and Gatzek, 2006), and would have forced the increase in pH during the initial 14 day period. Pore-water Fe^{III} was not detected, suggesting that Fe(III)-reduction occurred at the schwertmannite surface.

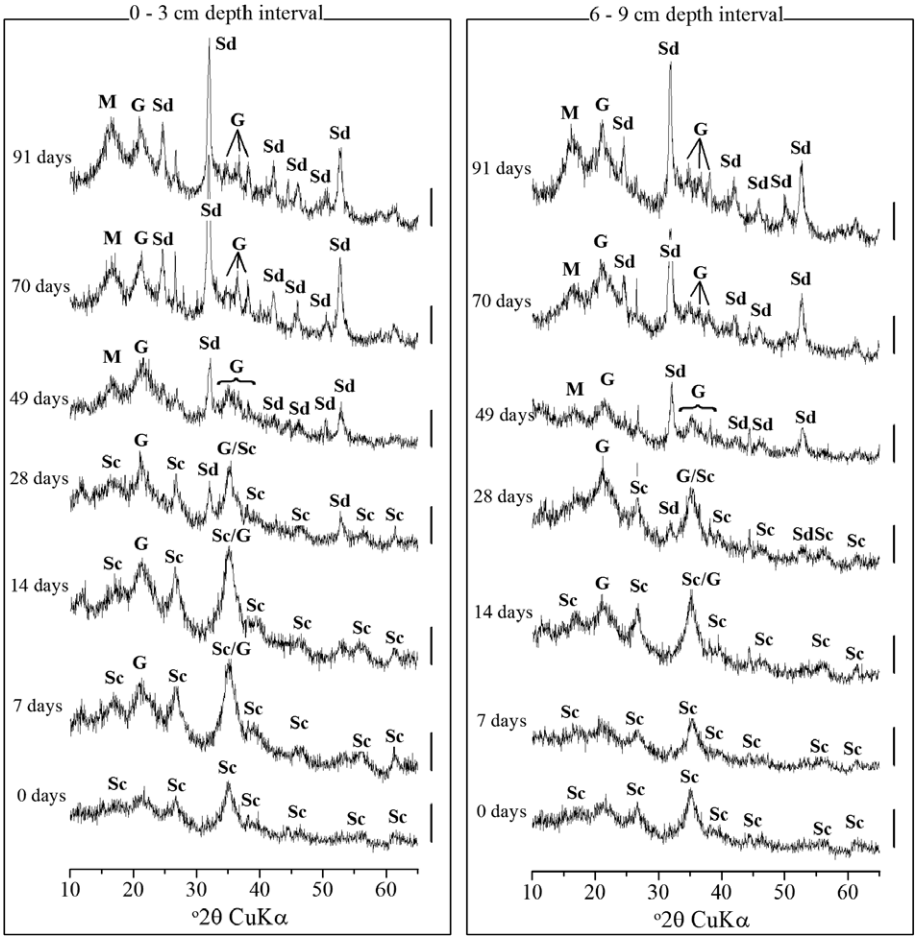

Fig. 1. X-ray diffractograms of material from two representative depth intervals showing temporal variations in mineralogy during waterlogging of schwertmannite-rich material. Peaks are denoted as Sc—schwertmannite, G—goethite, Sd—siderite, and M—nanoparticulate mackinawite. The scale bars represent 150 cps.

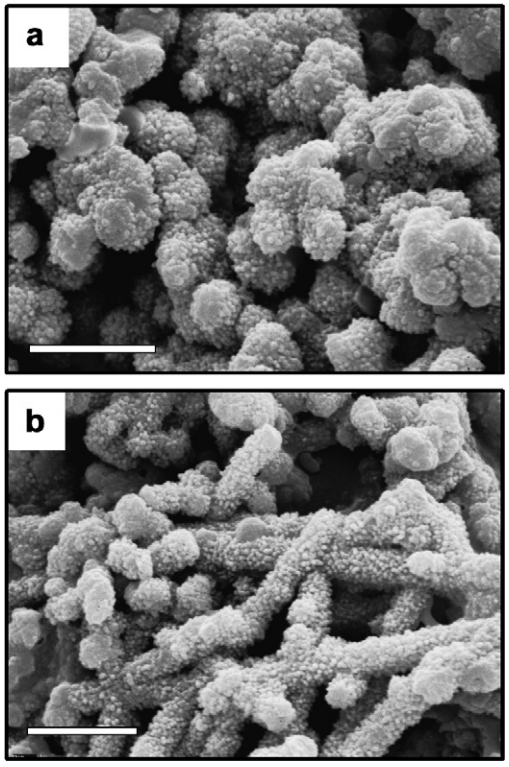

Fig. 2. Electron photomicrographs of schwertmannite in the initial sample, as spherical (a) or rod-shaped (b) aggregates. The bar denotes 2 μm.

Freshwater ponding and twice-weekly surface water replacements produced a strong depth-dependent gradient in the concentrations of major ions (Figs. 3 and 4). For example, the pore-water Cl concentration at 3 days post-inundation was 106 mM in the 0–3 cm depth interval compared to 406 mM in the 15–18 cm depth interval (Fig. 4). The relatively rapid decreases in pore-water Cl, Ca, K, Mg and Na concentrations in the near-surface depth intervals are attributable to diffusive flux of these components to the overlying surface water. The pore-water Fe^{II} and SO_4 concentrations were also substantially lower in the near-surface depth intervals (Fig. 3), which is consistent with diffusive losses to the surface water. It is important to note that diffusive losses of Fe and SO_4 (via twice-weekly surface-water replacement) accounted for decreases of <1% in the total Fe and S content of the columns.

The rate of initial pH increase, due to reductive-dissolution of schwertmannite, also varied with depth in the columns. In the near surface depth intervals (0–9 cm), pH increased to pH ~6.5 within the initial 14 days (Fig. 3). In contrast, pH >6 was attained more slowly (within 28 days) at greater depths in the columns. Pore-water in the near surface depth intervals experienced diffusive losses of Fe^{II} to the surface water within the initial 7 days (Fig. 3). During this period, diffusive flux caused lower aqueous Fe^{II} concentrations near the interface with the overlying water, compared with higher Fe^{II} in deeper material (Fig. 3). Accumulation of aqueous Fe^{II} is known to slow the reduction of Fe(III), due to passivation of Fe(III)-oxide surfaces by adsorbed Fe^{II} (Roden and Urrutia, 1999). This suggests that the higher pore-water Fe^{II} concentrations towards the column base may have somewhat slowed schwertmannite reduction, and consequently also slowed the associated pH increase.

The relatively high aqueous Fe^{II} and alkalinity concentrations (Fig. 3), resulting from schwertmannite reduction, suggest the possible precipitation of siderite ($FeCO_{3(s)}$):

$$Fe^{2+} + HCO_3^- \rightleftharpoons FeCO_{3(s)} + H^+ \quad (2)$$

Geochemical modeling, using MINTEQA2, showed that all depth intervals were supersaturated with regard to siderite by 1–3 orders of magnitude by day 14. This degree of supersaturation persisted over the 91 day column experiment, which reflects kinetic constraints on siderite precipitation. Slow siderite precipitation kinetics were also observed by Jensen et al. (2002), who found similar degrees of supersaturation within the initial 100 days of siderite precipitation from supersaturated solutions. The XRD data provide direct evidence for siderite from day 28 onwards (Fig. 1), with siderite existing as relatively large (5–10 μm) spherical particles (Fig. 5). The increase in oxalate-extractable Fe(II) from 318 μmol g^{-1} to ~1000 μmol g^{-1} over the duration of the 91 day experiment can be largely attributed to accumulation of siderite (Fig. 6).

In addition to Fe(III)-reduction, the bacterial reduction of schwertmannite-derived SO_4 may also be an important terminal electron accepting process. Bacterial dissimilatory SO_4-reduction can be expressed as (where acetic acid represents a variety of utilizable organic electron donating substances):

$$CH_3COOH + SO_4^{2-} \rightarrow 2HCO_3^- + H_2S \quad (3)$$

Pore-water S^{-II} is a major product of SO_4-reduction, yet was undetectable (<1 μM) throughout the column experiment. The relative rate of S^{-II} formation was therefore slower than its loss from the pore-water. This is consistent with rapid precipitation of the Fe(II)-monosulfide mineral, nanoparticulate mackinawite (tetragonal FeS) (Rickard, 1995). This mineral (which was often termed "amorphous FeS" in earlier literature; Rickard and Morse, 2005) forms within seconds at near-neutral pH when solutions of Fe^{II} and S^{-II} are mixed according to:

$$Fe^{2+} + H_2S \rightarrow FeS_{(s)} + 2H^+ \quad (4)$$

The pH- and Fe^{2+}-dependent solubility of $H_2S_{(aq)}$ in rapid equilibrium with nanoparticulate mackinawite is described by (Rickard, 2006):

$$\log(H_2S) = \log K_{FeS} - \log(Fe^{2+}) - 2pH \quad (5)$$

where $\log K_{FeS} = 3.5$ (Rickard, 2006). Under the observed pore-water conditions (i.e. pH 6.5 and activity of $Fe^{2+} > 10^{-3}$), the solubility of $H_2S_{(aq)}$ is <0.5 μM in equilibrium with nanoparticulate mackinawite. The concentration of $H_2S_{(aq)}$ would be even lower if other Fe-sulfide minerals (e.g. crystalline mackinawite (FeS), greigite (Fe_3S_4) or pyrite) controlled $H_2S_{(aq)}$ solubility.

In addition to $H_2S_{(aq)}$, pore-water S^{-II} may also include contributions from HS^- as well as aqueous $FeS^0_{(aq)}$ species. Below pH 6.5, the abundance of HS^-

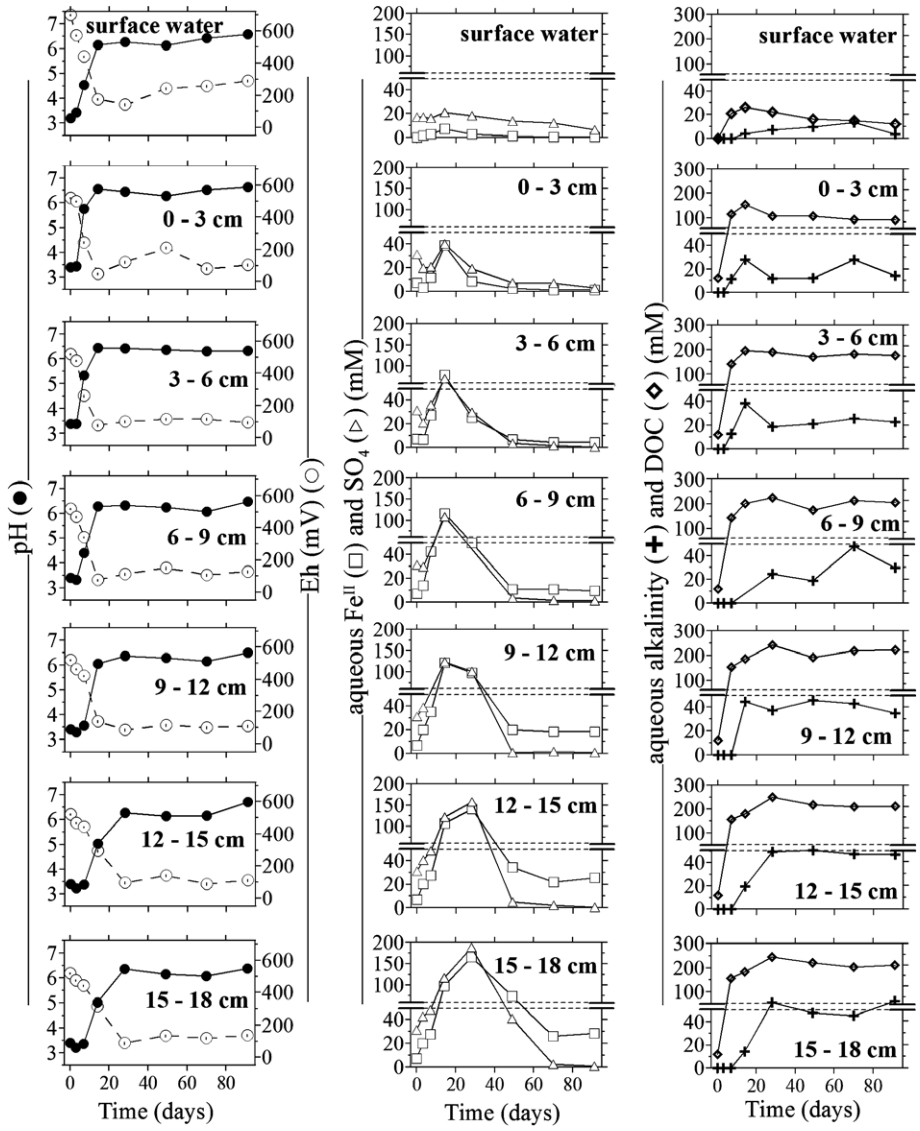

Fig. 3. Variations in pH, Eh, Fe^{II}, SO_4, alkalinity and DOC during waterlogging of schwertmannite-rich material. Data points are the means of duplicate analyses (the deviation between duplicate analyses was <10%).

becomes negligible compared to $H_2S_{(aq)}$. In contrast, the $FeS^0_{(aq)}$ species may contribute significantly to pore-water S^{-II} between approximately pH 6–6.5. Rickard (2006) estimated the intrinsic solubility of nanoparticulate mackinawite as:

$$FeS_{(s)} \rightarrow FeS^0_{(aq)} \quad (\log K = -5.7) \tag{6}$$

This implies that, at equilibrium with nanoparticulate mackinawite, $FeS^0_{(aq)}$ should be present at ~2 μM. The observation that pore-water S^{-II} concentrations were <1 μM indicates that formation of $FeS^0_{(aq)}$ was inhibited or that $FeS^0_{(aq)}$ was consumed by subsequent reactions.

Elemental S was the initial reduced inorganic S phase to accumulate at all depths in the columns (Fig. 7). This is consistent with oxidation of H_2S by Fe(III)-oxides (Rickard, 1974; Yao and Millero, 1996), such as goethite:

$$2\alpha FeOOH_{(s)} + H_2S + 4H^+ \rightarrow 2Fe^{2+} + S^0_{(s)} + 4H_2O \tag{7}$$

Observation of in-situ sediment geochemistry in waterways associated with acid sulfate soils indicates that $S^0_{(s)}$ may also form via H_2S oxidation by schwertmannite (Burton et al., 2006a,d):

$$Fe_8O_8(OH)_6(SO_4)_{(s)} + 4H_2S + 14H^+ \rightarrow 8Fe^{2+} + 4S^0_{(s)} + SO_4{}^{2-} + 14H_2O \tag{8}$$

Fig. 7 shows that $S^0_{(s)}$ was a major reductive mineralization product formed during the column experiment. However, the nature of $S^0_{(s)}$ formed via Eqs. (7) and (8) is poorly understood. Of the elements, $S^0_{(s)}$ exhibits the largest number of solid-phase allotropes, with most consisting of unbranched cyclic molecules with ring sizes ranging from 6 to 20 atoms (Steudel and Eckert, 2004). Polymeric $S^0_{(s)}$ allotropes, comprising chains in a random coil or helical conformation, are also known to occur (Steudel and Eckert, 2004).

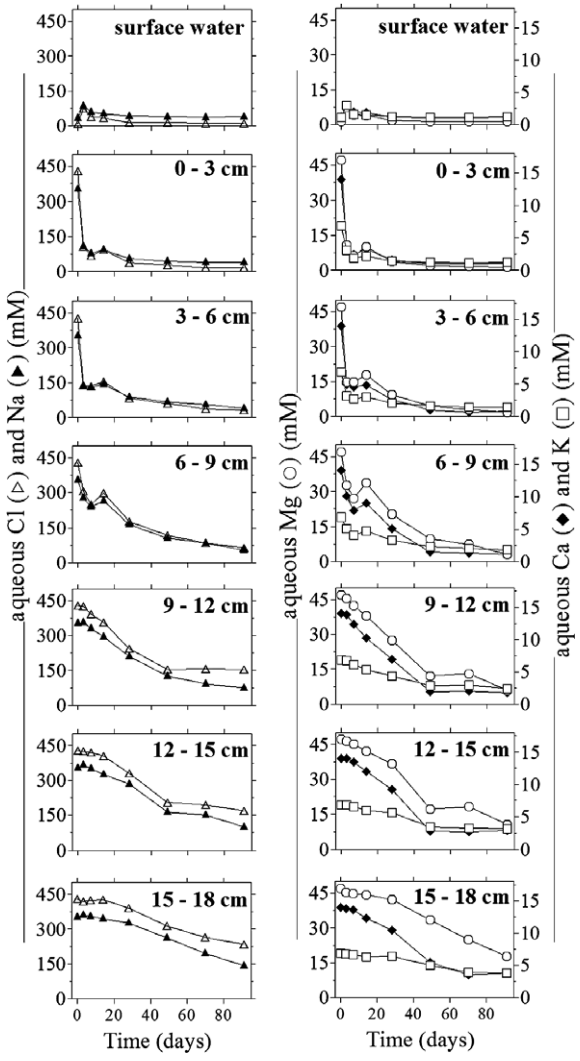

Fig. 4. Variations in the aqueous concentrations of Cl, Na, Mg, Ca and K during waterlogging of schwertmannite-rich material. Data points are the means of duplicate analyses (the deviation between duplicate analyses was <10%).

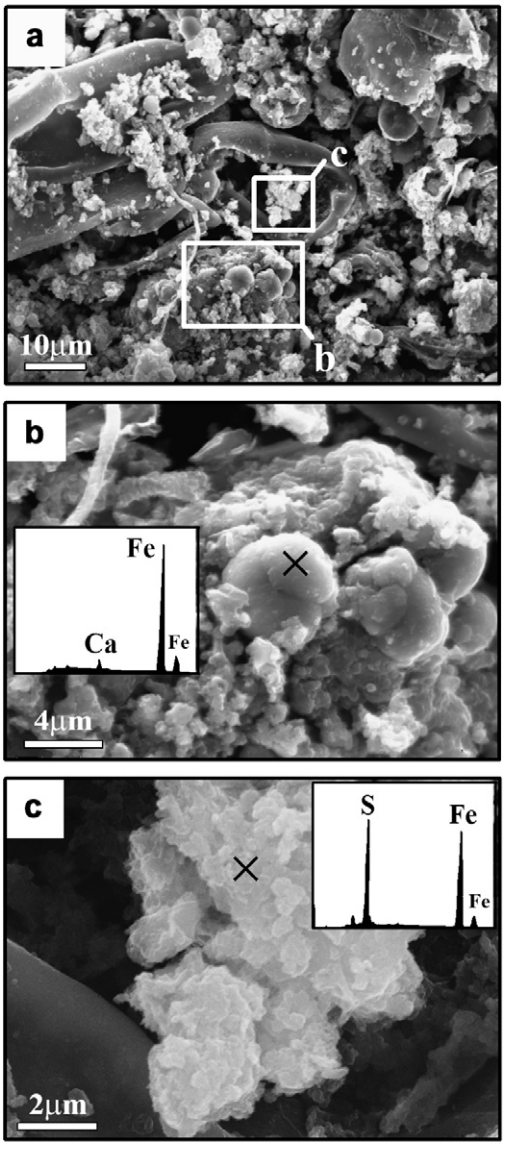

Fig. 5. Electron photomicrographs for material sampled at 91 days (0–3 cm depth) in the long-term column experiment (a), with EDX spectra for siderite (b) and nanoparticulate mackinawite (c).

Accumulation of AVS commenced at 28–49 days depending on depth within the columns (Fig. 7). By 91 days, AVS had increased to a maximum of 237 μmol g^{-1} in the 0–3 cm depth interval (Fig. 7). Similar AVS concentrations have been reported in accumulations of ''monosulfidic black ooze'' in waterways and floodplains of acidified coastal lowlands (Sullivan et al., 2002; Bush et al., 2004; Burton et al., 2006a,c). Sedimentary AVS has also been reported as a product of schwertmannite-reduction in acidic, coal-mine pit lakes (Peine et al., 2000; Blodau and Knorr, 2006). It should be noted that although AVS has been frequently observed, the mineralogical components of AVS (which include a wide range of potential phases) have been rarely identified (Rickard and Morse, 2005).

The accumulation of AVS was accompanied by development of a broad XRD peak at ~17°2θ Cu Kα (i.e. a *d*-value of ~0.5 nm) (Fig. 1). This XRD peak is consistent with the spacing between Fe-sheets (001 Bragg reflection) in the structure of mackinawite (Rickard and Morse, 2005). Mackinawite is a tetragonal Fe(II) monosulfide that is quantitatively recovered by the AVS extraction procedure employed in the present study. In order to verify that mackinawite was the cause of the peak at ~0.5 nm, an AVS-rich sample (0–3 cm, 91 days inundation) was aerated for 24 h in deionised water. Aeration caused complete oxidative loss of AVS (and therefore loss of any mackinawite), with differential XRD demonstrating disappearance of the ~0.5 nm peak. The presence of a single broad XRD peak at ~0.5 nm is characteristic of nanoparticulate mackinawite, which typically lacks the other XRD peaks of bulk mackinawite (Wolthers et al., 2003; Rickard and Morse, 2005). Material meeting the mackinawite composition (i.e. stoichiometric $FeS_{(s)}$; Rickard et al., 2006) was identified by

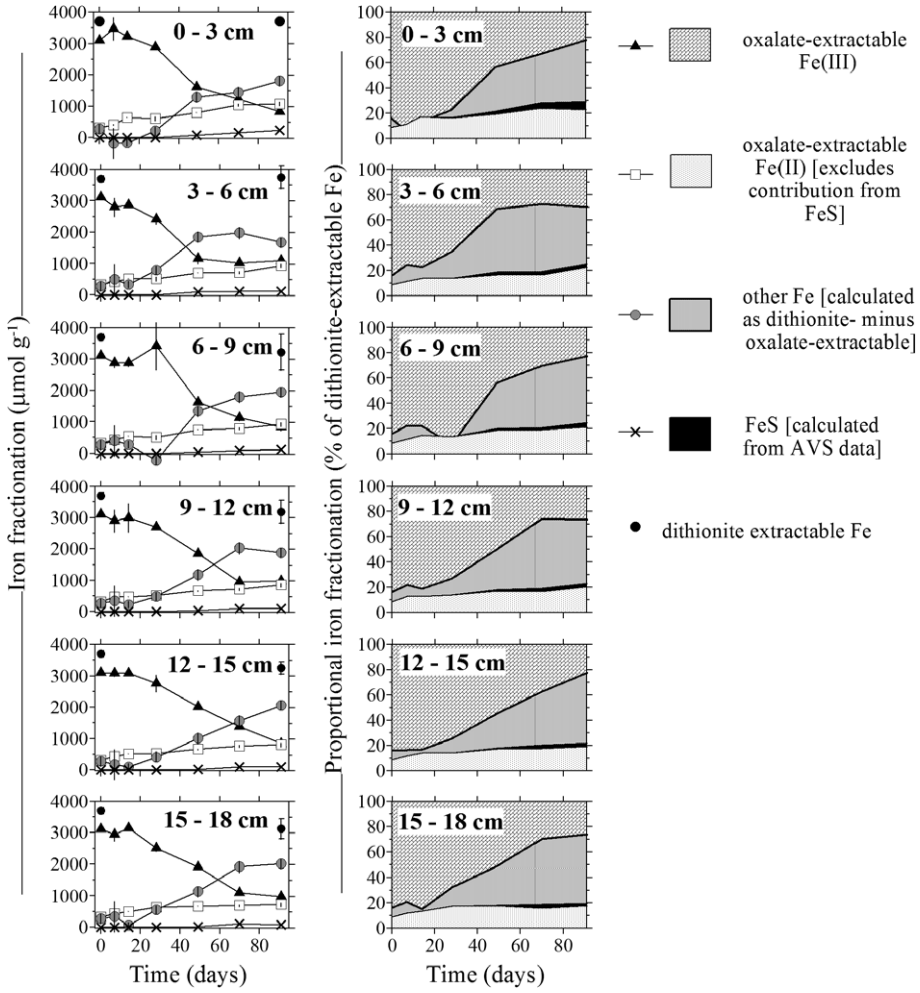

Fig. 6. Variations in solid-phase Fe fractions during waterlogging of schwertmannite-rich accumulations. Dithionite extractable Fe concentrations did not change significantly during the experiment and are therefore presented for 0 days and 91 days only. The proportional Fe fractionation data represents the abundance of each Fe fraction relative to the dithionite extractable Fe concentration. Pyrite–Fe comprised <1% of total Fe and is not presented. Data points are the means of duplicate analyses, with error bars denoting ±1 standard deviation (error bars are presented only for data points having a relative standard deviation >5%).

SEM–EDX analysis as aggregates of sub-micron size crystals (Fig. 5). This material was further examined by TEM, with SAED confirming the presence of nanoparticulate mackinawite (Fig. 8). Overall, the results demonstrate that nanoparticulate mackinawite was the principal Fe(II)-monosulfide mineral resulting from reductive transformation of the schwertmannite- and organic-rich soil material described here.

Nanoparticulate mackinawite is metastable and tends to be replaced by pyrite (Rickard and Morse, 2005). Pyrite was detectable from day 28 onwards in the long-term column experiment, with the final 91-day pyrite–S contents spanning 23 ± 2 μmol g^{-1} (0–3 cm depth) to 14 ± 2 μmol g^{-1} (15–18 cm depth). The pyrite–S contents increased from days 28–91 at rates of approximately 0.2–0.3 μmol g^{-1} day^{-1} (determined by linear regression for each depth interval; all r^2 values >0.9). These observed rates of pyrite formation can be compared to theoretical rates using rate laws determined from abiotic experiments. The rate of abiotic pyrite formation can be expressed as (Rickard and Morse, 2005):

$$\frac{d(FeS_{2(s)})}{dt} = k_1(FeS_{(s)})^2(S^0_{(s)})(S^{-II})\{H^+\} + k_2(FeS_{(s)})(H_2S) \quad (9)$$

where $k_1 = 350$ L^3 mol^{-3} s^{-1} and $k_2 = 10^{-4}$ L mol^{-1} s^{-1}; $\{H^+\}$ is the H^+ activity; $(FeS_{(s)})$, $(S^0_{(s)})$, (S^{-II}) and $(H_2S_{(aq)})$ are the molar concentrations (mol L^{-1}) of $FeS_{(s)}$, $S^0_{(s)}$, S^{-II} and $H_2S_{(aq)}$, respectively (Rickard and Morse, 2005). By using the sample water content and sample density to convert from volumetric units (L^{-1}) to gravimetric units (g^{-1}) and using conditions relevant to the onset of pyrite formation in the column experiment (i.e. pH 6.5; $(FeS_{(s)}) = (S^0_{(s)}) = 20$ μmol g^{-1}; $(H_2S) = 10^{-7}$ M), the calculated abiotic pyrite–S formation rate is ~0.00002 μmol g^{-1} day^{-1}. This abiotic rate is ~4 orders of magnitude less than the observed rates (i.e. 0.2–0.3 μmol g^{-1} day^{-1}). Canfield et al. (1998) and Carey and

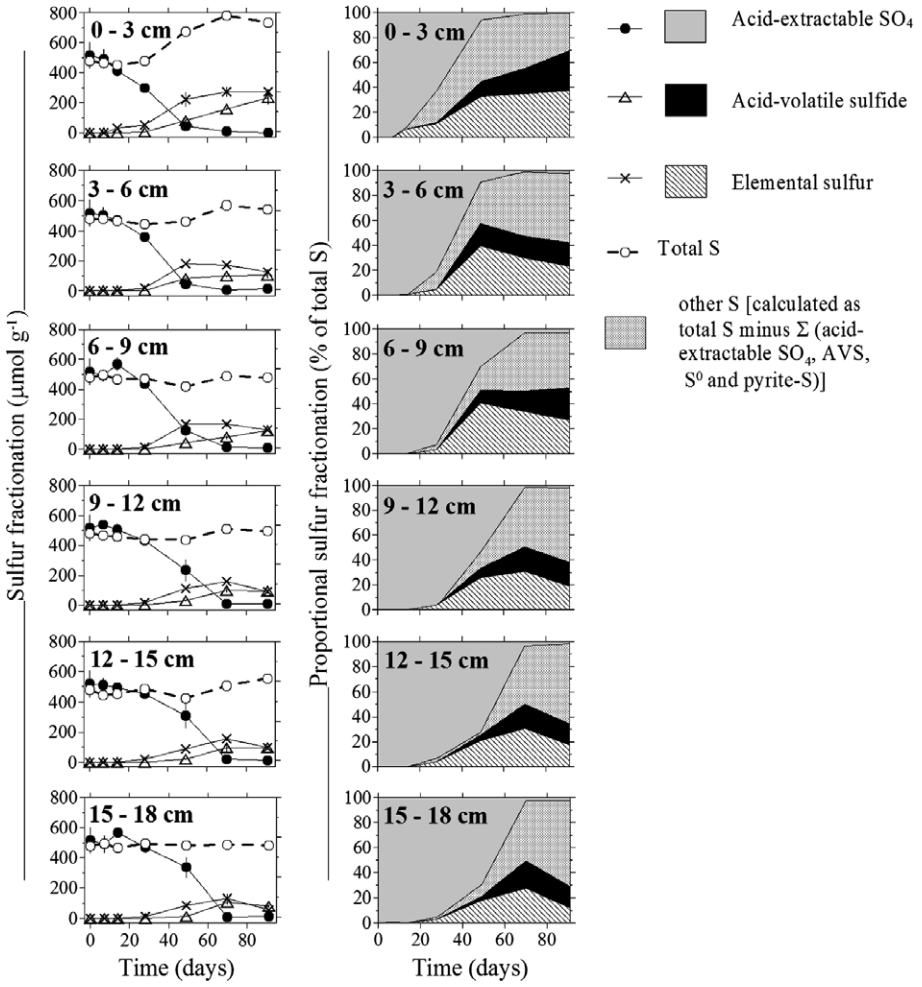

Fig. 7. Variations in solid-phase S fractions during waterlogging of schwertmannite-rich soil material. The proportional S fractionation data represents the abundance of each S fraction relative to the measured total S concentrations. The absolute pyrite–S concentrations (all data <22 μmol g^{-1}) and proportional pyrite–S abundances (all data <3% of total S) were quantitatively very minor and are not presented. Data points are the means of duplicate analyses, with error bars denoting ±1 standard deviation (error bars are presented only for data points having a relative standard deviation >5%).

Taillefert (2005) also found that measured pyrite formation rates exceeded calculated rates by several orders of magnitude. Canfield et al. (1998) suggested that the presence of bacterial surfaces greatly accelerated the rates of pyrite formation beyond that observed in abiotic experiments. This hypothesis is supported by Donald and Southam (1999) who observed bacterially catalysed nucleation of pyrite at the surface of sulfate-reducing bacteria.

Although pyrite formed much faster than expected for purely abiotic reactions, pyrite comprised only a very minor proportion (<1% of total Fe, <3% of total S) of the mineralisation products observed at day 91. This result contrasts with the typical dominance of pyrite, formed as a result of Fe(III)- and SO_4-reduction, in estuarine and marine sediments (Rickard and Morse, 2005; Burton et al., 2006e). However, the low levels of pyrite formation during the present study concur with field observations regarding the persistence of Fe(II)-monosulfides in Fe-rich sediments (Sullivan et al., 2002; Bush et al., 2004; Burton et al., 2006a,c). It is also consistent with the kinetics of pyrite formation, which show a direct dependence of the pyrite formation rate on the $H_2S_{(aq)}$ concentration (Eq. (9)). The high pore-water Fe^{II} concentrations produced by schwertmannite reduction prevent the accumulation of pore-water $H_2S_{(aq)}$ (via nanoparticulate mackinawite precipitation) and thereby kinetically retard pyrite formation. This explains the relative dominance of meta-stable nanoparticulate mackinawite over thermodynamically-favoured pyrite.

The XRD data demonstrate formation of substantial amounts of goethite within the initial 28 day period (Fig. 1). The importance of goethite formation is evident from significant increases with time in the intensity of the (1 1 0) Bragg reflection for goethite (i.e. ~21°2θ Cu Kα) (and the appearance towards the end of the experiment of the less intense (1 3 0), (0 2 1) and (1 1 1) goethite reflections at 33.3°2θ, 34.7°2θ and 36.6°2θ Cu Kα, respectively) (Fig. 1). Schwertmannite is known to transform to goethite via a dissolution/precipitation process according to (Bigham et al., 1996a):

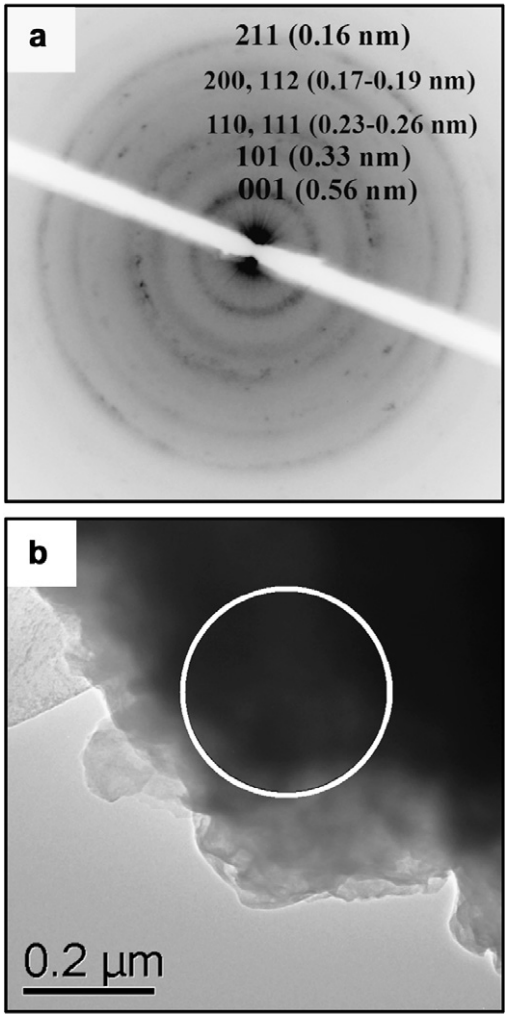

Fig. 8. Selected area electron diffraction pattern (a) and transmission electron photomicrograph (b) for clusters of mackinawite crystals formed in the column experiment (specimen from the 0 to 3 cm depth; 91 days post inundation). The *d*-spacings shown in (a) correspond to mackinawite with slight expansion along the *c*-axis. This feature is typical for nanoparticulate mackinawite and is discussed in detail by Wolthers et al. (2003). The circle shown in (b) denotes the area from which the electron diffraction data shown in (a) was collected.

$$Fe_8O_8(OH)_6SO_{4(s)} + 2H_2O \rightarrow 8\alpha FeOOH_{(s)} + SO_4^{2-} + 2H^+ \quad (10)$$

The formation of goethite within the initial 28 days is significant, as previous research has shown that transformation of schwertmannite to goethite at pH 6–7 occurs much slower than observed here. For example, Regenspurg et al. (2004) and Jonsson et al. (2005) found comparable XRD results only after aging periods of hundreds of days under oxic conditions.

Oxalate extractions have been used to quantify the relative abundance of schwertmannite versus goethite (Bigham et al., 1996a; Dold, 2003; Gagliano et al., 2004). This is valid for samples containing negligible Fe(II), in which oxalate-extractions yield only very minor goethite recovery yet complete extraction of schwertmannite (Dold, 2003). However, goethite is partially extractable by oxalate in the presence of appreciable Fe(II), and therefore in the present study oxalate-extractable Fe(III) is not a quantitative measure of schwertmannite versus goethite abundance. Taking this into consideration, the "other Fe" fraction (calculated as dithionite-extractable Fe minus oxalate-extractable Fe) shown in Fig. 6 can be interpreted as reflecting goethite alone. This interpretation is justified as goethite was the only Fe mineral present that would have been partially recovered by oxalate-extraction, yet completely recovered by dithionite-extraction (i.e. present as "other Fe"; Fig. 6). The increasing proportion of "other Fe" throughout the experiment qualitatively reflects the transformation of schwertmannite to goethite (Fig. 6). It is important to note, however, that this "other Fe" fraction underestimates actual goethite abundance, as a significant proportion of goethite would also be included in the oxalate-extractable Fe(III) fraction of these materials. The implication is that schwertmannite transformed to goethite even more rapidly and extensively than suggested by the "other Fe" data (Fig. 6).

The "other S" fraction increased during the column experiment from 0% of total S initially to between 30% and 68% of total S at 91 days (Fig. 7). The XRD and Fe fractionation data show that goethite was the major diagenetic Fe phase to form during the column experiment (Figs. 1 and 6). In SO_4-rich environments, goethite can contain significant (10–15%) amounts of incorporated SO_4 (Webster et al., 1998; Kumpulainen et al., 2007). As described previously (see Section 2), a considerable proportion of well-ordered goethite is not recovered by the acid extraction procedure (i.e. 6 M HCl/0.1 M ascorbic acid) employed in the present study. Accordingly, any SO_4 bound within such goethite would also not be recovered as acid-extractable SO_4, and would instead be included as "other S". The observed increases in "other S" during the column experiment may therefore largely reflect the increasing importance of SO_4 incorporation within non-acid-extractable goethite (Fig. 7).

3.3. Short-term abiotic batch experiment

The data from the column experiment show that goethite formation represented an important sink for both Fe and S. This can be attributed to the relatively rapid and extensive transformation of schwertmannite to goethite. Previous research has shown that Fe^{II} catalyses transformation of ferrihydrite to more crystalline phases, such as goethite and lepidocrocite (Hansel et al., 2005; Pedersen et al., 2005). A similar Fe^{II}-catalysed transformation process may also occur for schwertmannite; thereby potentially explaining the rapidity and extent of goethite formation during the column experiment. Schwertmannite, however, commonly forms and persists in pH 3–4 waters that are relatively rich in Fe^{II} (Bigham et al., 1996a,b; Yu et al., 1999; Regenspurg et al., 2004; Acero et al., 2006). Transformation of schwertmannite by reaction with Fe^{II} may, therefore, seem inconsistent with the co-occurrence of schwertmannite and Fe^{II} in acidic waters. Then again, at low pH there is little ten-

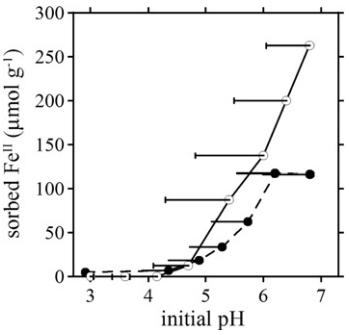

Fig. 9. pH-dependent sorption of Fe^{II} to synthetic schwertmannite (24 h reaction period). Open and filled circles denote initial aqueous Fe^{II} concentrations of 10 mM and 1 mM, respectively. Sorbed Fe^{II} concentrations corresponding to 100% sorption are 1250 μmol g^{-1} and 125 μmol g^{-1} for initial aqueous Fe^{II} concentrations of 10 mM and 1 mM, respectively. The horizontal bars show the pH decrease during the 24 h equilibration period.

dency for interactions between schwertmannite and Fe^{II}, given that schwertmannite has a pH 7.2 point of zero charge (Jonsson et al., 2005). The results presented in Fig. 9 are consistent with this assertion and demonstrate negligible levels of Fe^{II} sorption to schwertmannite at pH <5.

Sorption of Fe^{II} to schwertmannite was increasingly significant at pH >5 (Fig. 9). The corresponding XRD data demonstrate that Fe^{II} sorption catalysed the rapid (within 24 h) transformation of schwertmannite to more crystalline phases (Figs. 10 and 11). The degree of this transformation, as evident from XRD peak intensity, was more substantial with increasing pH (Fig. 10) and with increasing Fe^{II} concentration (Fig. 11). In experimental systems buffered at pH 6.5, the main products were lepidocrocite and goethite when 0.05 M MES/MOPS was used as the buffer and goethite alone when 0.05 M HCO_3 was used (Fig. 11). The absence of lepidocrocite in the presence of HCO_3 is expected as the HCO_3^- anion is known to inhibit lepidocrocite crystallization (Cornell and Schwertmann, 2003; Hansel et al., 2005). Additionally, goethite formation was somewhat retarded in the presence of HCO_3 (Fig. 11), as has been observed for Fe^{II}-catalysed transformation of ferrihydrite (Hansel et al., 2005). Overall, the data show clearly that (at near-neutral pH) Fe^{II} can rapidly catalyse the transformation of schwertmannite to more crystalline phases.

Aqueous Fe^{II} concentrations and other experimental conditions used in the short-term batch experiments were comparable to those observed in the long-term column experiment. The dominance of goethite as a reductive mineralization product in the column experiment can therefore be largely attributed to the Fe^{II}-catalysed schwertmannite transformation pathway. Following research into ferrihydrite behaviour (Pedersen et al., 2005), we hypothesize that this schwertmannite transformation pathway is related to electron exchange between sorbed Fe(II) and Fe(III) at the schwertmannite surface. The more labile nature of the resulting Fe(II)–O bond at the schwertmannite surface compared to the former Fe(III)–O bond would destabilize the schwertmannite structure. This leads to schwertmannite dissolution and subsequent precipitation of more stable phases, such as goethite.

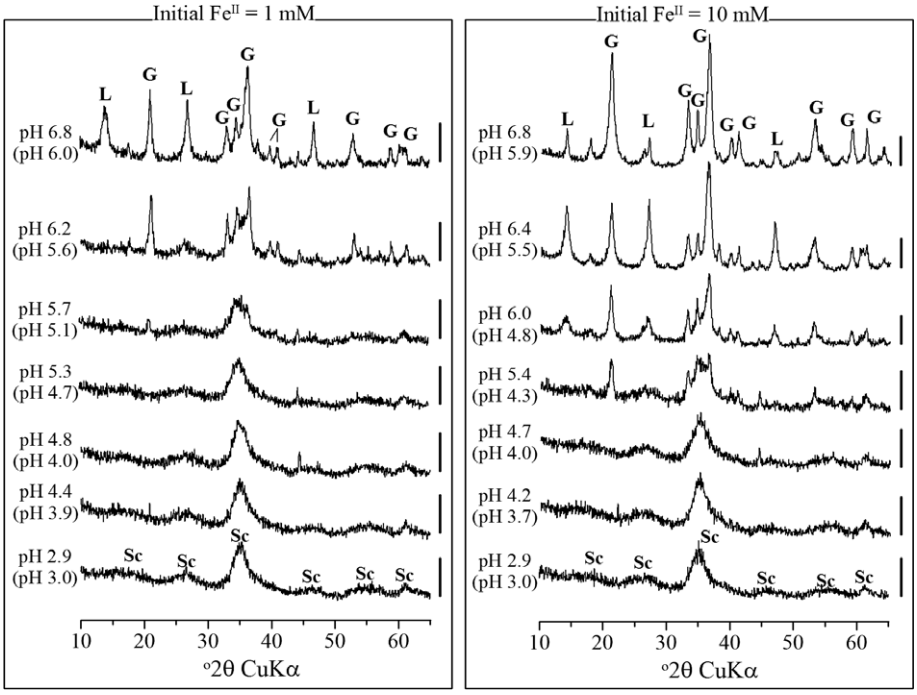

Fig. 10. X-ray diffractograms showing the effect of pH on the mineralogy resulting from schwertmannite-Fe^{II} interactions (24 h reaction period). The initial pH is shown above the final 24 h pH value (shown in brackets). The scale bars denote 150 cps. Labels are Sc—schwertmannite, L—lepidocrocite and G—goethite.

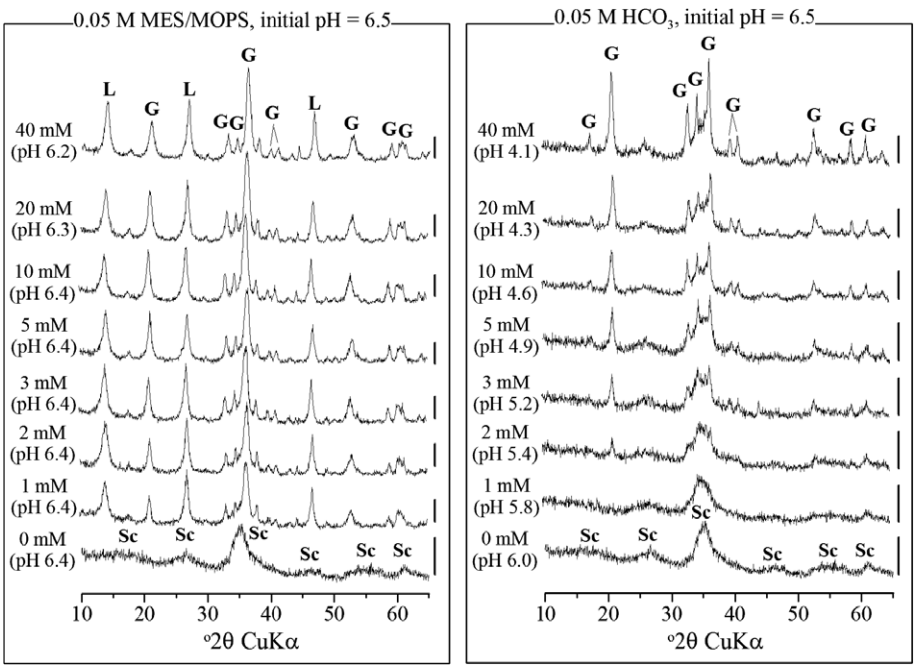

Fig. 11. X-ray diffractograms showing the effect of Fe^{II} loading on the mineralogy resulting from schwertmannite-Fe^{II} interactions (24 h reaction period). For all treatments the initial pH was 6.5 and the final (24 h) pH value is shown in brackets. The scale bars denote 150 cps. Labels are Sc—schwertmannite, L—lepidocrocite and G—goethite.

3.4. A partial equilibrium interpretation of Fe(III)- versus SO_4-reduction

The suite of Fe and S phases formed during the long-term column experiment are either direct (i.e. siderite, $S^0_{(s)}$, mackinawite and pyrite) or indirect (i.e. goethite) products of bacterial Fe(III)- and/or SO_4-reduction. The spatial and temporal distribution of Fe(III)- and SO_4-reduction is often interpreted by comparing the standard state Gibbs free energy for the overall processes (Stumm and Morgan, 1996). Accordingly, SO_4-reduction is not expected to occur substantially until near-complete reduction of Fe(III). This is inconsistent with the results described here, which show that accumulation of SO_4-reduction products occurred in the presence of abundant Fe(III) (Figs. 1, 6 and 7).

Postma and Jakonsen (1996) argue that the overall process of reaction between organic matter and Fe(III) or SO_4 as electron acceptors can be conceptualized as two steps. Firstly, a slow, overall rate-determining fermentative step where fermenting bacteria produce simple organic molecules (e.g. acetate, lactate) for which Fe(III)- and SO_4-reducing bacteria compete. Secondly, a fast electron accepting step, such as Fe(III)- or SO_4-reduction, that approximates equilibrium. Postma and Jakonsen (1996) therefore proposed a partial equilibrium approach to understand the distribution of terminal electron accepting processes in reducing environments. This approach has subsequently been applied successfully to interpret redox zonation in Fe(III)-rich sediments of coal mining lakes (Blodau and Peiffer, 2003).

In the present study, we derive a modification of the partial equilibrium approach presented by Blodau and Peiffer (2003). The general approach involves modeling the difference in energy yields between reduction of Fe(III) and SO_4. This is then compared with the spatial and temporal variations in accumulation of SO_4-reduction products in the long-term column experiment. It is acknowledged that the presented model does not consider micro-niche effects nor the intricacies of microbial physiology or ecology. Nevertheless, microbial activities must be related to the energy yield of microbially-mediated electron accepting processes and therefore the model provides a useful theoretical foundation for the prediction of the energetic favourability of Fe(III)- versus SO_4-reduction.

On an electron equivalent basis, the reduction of SO_4 can be expressed as:

$$\frac{1}{8}SO_4^{2-} + \frac{5}{4}H^+ + e^- \rightarrow \frac{1}{8}H_2S + \frac{1}{2}H_2O \quad (11)$$

The reduction of goethite-derived Fe(III) can be expressed as:

$$\alpha FeOOH_{(s)} + e^- + 3H^+ \rightarrow Fe^{2+} + 2H_2O \quad (12)$$

Likewise, reduction of schwertmannite-derived Fe(III) can be expressed as:

$$FeO(OH)_{6/8}(SO_4)_{1/8(s)} + e^- + \frac{11}{4}H^+ \rightarrow Fe^{2+} + \frac{1}{8}SO_4^{2-} + \frac{7}{4}H_2O \quad (13)$$

The difference in the free energy change of reaction (ΔG_r) between reduction of goethite-derived Fe(III) versus reduction of SO_4 as terminal electron accepting processes can therefore be expressed as:

$$\Delta G_{r,(Eq.(12))} - \Delta G_{r,(Eq.(11))} = \Delta G^0_{r,(Eq.(12))} - \Delta G^0_{r,(Eq.(11))} + RT2.3\left\{\log(Fe^{2+}) + \frac{1}{8}\log(SO_4{}^{2-}) - \frac{1}{8}\log(H_2S) + \frac{7}{4}pH\right\} \quad (14)$$

This equation was applied by Blodau and Peiffer (2003) to also describe the relative advantage of SO_4-reduction versus reduction of schwertmannite-derived Fe(III). However, it is evident from Eq. (13) that a more appropriate expression for the difference in energy yield between SO_4-reduction and reduction of schwertmannite-derived Fe(III) is:

$$\Delta G_{r,(Eq.(13))} - \Delta G_{r,(Eq.(11))} = \Delta G^0_{r,(Eq.(13))} - \Delta G^0_{r,(Eq.(11))} + RT2.3\left\{\log(Fe^{2+}) + \frac{2}{8}\log(SO_4{}^{2-}) - \frac{1}{8}\log(H_2S) + \frac{3}{2}pH\right\} \quad (15)$$

The standard state free energy of reaction (ΔG^0_r) values for Eqs. (11) and (12) were calculated using standard state free energies of formation (ΔG^0_f) for $SO_4{}^{2-}$ (-744.6 kJ mol^{-1}), $H_2S_{(aq)}$ (-27.87 kJ mol^{-1}), $H_2O_{(l)}$ (-237.18 kJ mol^{-1}) and goethite (-488.6 kJ mol^{-1}) presented in Stumm and Morgan (1996). The ΔG^0_f for Fe^{2+} (-78.9 kJ mol^{-1}) selected by the National Bureau of Standards (Wagman et al., 1968; and subsequently presented in Stumm and Morgan, 1996) has been applied in previous work examining Fe(III)- versus SO_4-reduction (Blodau and Peiffer, 2003). However, this early ΔG^0_f value for Fe^{2+} has now been discarded due to intrinsic oxidation in the primary experiments. In our calculations, we used the revised ΔG^0_f value for Fe^{2+} (-90.5 kJ mol^{-1}) as described by Parker and Khoakovskii (1995). Using these ΔG^0_f values and expressing as electron equivalents yields $\Delta G^0_r = -29$ kJ eq^{-1} for SO_4-reduction and $\Delta G^0_r = -76$ kJ eq^{-1} for reduction of goethite-derived Fe(III).

The calculation of ΔG_r for reduction of schwertmannite-derived Fe(III) is not as straightforward, as there is uncertainty regarding the ΔG^0_f value of schwertmannite. Majzlan et al. (2004) report a ΔG^0_f value for schwertmannite (as $FeO(OH)_{6/8}(SO_4)_{1/8}$) of -518 kJ mol^{-1} based on measurement of enthalpy of formation via acid calorimetry and an estimate of the standard entropy. However, the applicability of this ΔG^0_f value to natural environments is questionable, given that true thermodynamic equilibrium may never be attained due to the metastability of schwertmannite with regard to goethite. For example, field observations involving SO_4-rich waters consistently show that schwertmannite dominates over ferrihydrite only below about pH 4.5 (Bigham et al., 1996a; Yu et al., 1999; Murad and Rojik, 2003). In contrast, a ΔG^0_f value for schwertmannite of -518 kJ mol^{-1} indicates that, in the presence of such SO_4 concentrations, schwertmannite should occur instead of ferrihydrite up to about pH 7 (Majzlan et al., 2004).

The solubility constant for schwertmannite calculated from $\Delta G^0_f = -518$ kJ mol^{-1} (i.e $\log K_{sp} = \log(Fe^{3+})^8(SO_4{}^{2-})/(H^+)^{22} = 9.6$) is also inconsistent with the majority of reported K_{sp} values. Bigham et al. (1996a) found that $\log K_{sp} = 18 \pm 2.5$ best represented apparent schwertmannite solubility in the field. Regenspurg et al. (2004) and Sullivan and Bush (2004) confirmed that $\log K_{sp} = 18$ provided a very good fit to the pH-dependency of Fe^{III} solubility in natural waters associated with schwertmannite. Likewise, field data presented by Yu et al. (1999) show remarkable agreement with $\log K_{sp} = 18$. However, these authors assumed that all of their water samples were supersaturated with respect to schwertmannite and defined $\log K_{sp}$ based on the lowest observed ion activity product ($\log 10.5$), even though the majority of their data supported $\log K_{sp} = 18$ (see Figs. 5 and 6 in Yu et al., 1999). Furthermore, Regenspurg and Peiffer (2005) also arrived at $\log K_{sp} = 18$ from a 1 year dissolution experiment involving synthetic schwertmannite. An apparent solubility product of $\log K_{sp} = 18$ (although possibly not reflecting true equilibrium) implicitly accounts for the theoretical problem of schwertmannite metastability and consequently provides an accurate estimate of actual schwertmannite solubility. This $\log K_{sp}$ value yields $\Delta G^0_f = -500$ kJ mol^{-1} for schwertmannite (as $FeO(OH)_{6/8}(SO_4)_{1/8}$). This ΔG^0_f value agrees with $\Delta G^0_f = -501$ kJ mol^{-1} as calculated from the pore-water pH, Eh, and activities of Fe^{2+} and $SO_4{}^{2-}$ in the initial schwertmannite-rich sample used in the column experiment. In the present study we therefore have used $\Delta G^0_f = -500$ kJ mol^{-1} for schwertmannite (as $FeO(OH)_{6/8}(SO_4)_{1/8}$), which equates to $\Delta G^0_r = -99$ kJ eq^{-1} for reduction of schwertmannite derived Fe(III) (Eq. (13)).

In the Fe^{II}-rich material described here, $H_2S_{(aq)}$ was undetectable due to the pH- and Fe^{2+}-dependent solubility of nanoparticulate mackinawite. However, this problem (in terms of solving Eqs. (14) and (15)) can be overcome by estimating $H_2S_{(aq)}$ according to Eq. (5). This approach is valid because even though oxidation of $H_2S_{(aq)}$ to $S^0_{(s)}$ via Eqs. (7) and (8) is important in terms of S fate, the $H_2S_{(aq)}$ activity can still be assumed to be controlled by the rapid precipitation–dissolution of nanoparticulate mackinawite (Eq. (5)). Incorporating this estimate of $H_2S_{(aq)}$, the relative advantage of reduction of goethite-derived Fe(III) versus SO_4-reduction, under solubility equilibrium and Fe^{II}-rich conditions can be expressed as:

$$\Delta G_{r,(Eq.(12))} - \Delta G_{r,(Eq.(11))} = \Delta G^0_{r,(Eq.(12))} - \Delta G^0_{r,(Eq.(11))} + RT2.3\left\{\frac{9}{8}\log(Fe^{2+}) + \frac{1}{8}\log(SO_4{}^{2-}) + 2pH + \frac{1}{8}\log K_{FeS}\right\} \quad (16)$$

Likewise, the ΔG_r difference between reduction of schwertmannite-derived Fe(III) versus reduction of SO_4 can be expressed as:

$$\Delta G_{r,(Eq.(13))} - \Delta G_{r,(Eq.(11))} = \Delta G^0_{r,(Eq.(13))} - \Delta G^0_{r,(Eq.(11))} + RT2.3\left\{\frac{9}{8}\log(Fe^{2+}) + \frac{2}{8}\log(SO_4{}^{2-}) + \frac{7}{4}pH + \frac{1}{8}\log K_{FeS}\right\} \quad (17)$$

The results of these model calculations (using data from the column experiment) are presented in Fig. 12. The results show that within the initial 14 days in the column experiment there were marked decreases in the favourability of Fe(III)-reduction for Fe(III) derived from both schwert-

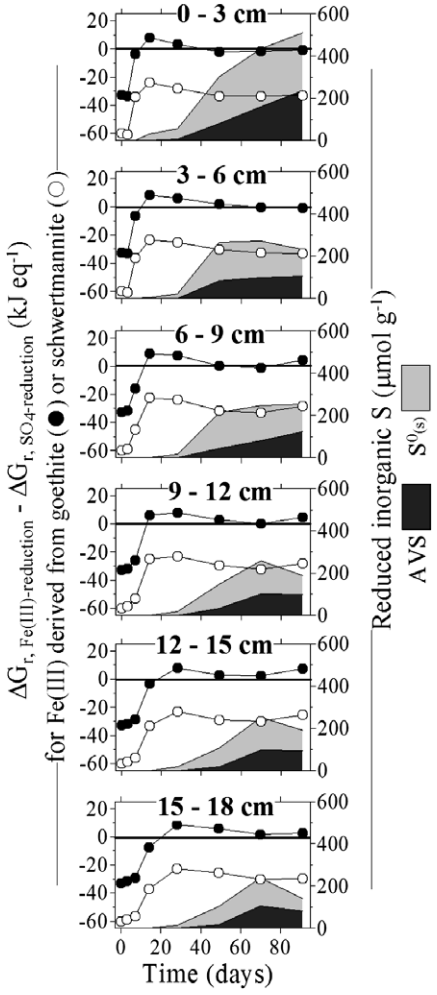

Fig. 12. Partial equilibrium interpretation of temporal and spatial variations in the relative energy yields for Fe(III)- versus SO_4-reduction during the column experiment. The difference in energy yields is shown for Fe(III) derived from either goethite or schwertmannite. The solid line (i.e. $\Delta G_{r,\ Fe(III)\text{-reduction}} - \Delta G_{r,SO_4\text{-reduction}} = 0$) indicates equivalent energy yields for both Fe(III)- versus SO_4-reduction. Reduction of Fe(III) is favoured below this line (i.e. $\Delta G_{r,\ Fe(III)\text{-reduction}} - \Delta G_{r,\ SO_4\text{-reduction}} < 0$), whereas reduction of SO_4 is favoured above the line (i.e. $\Delta G_{r,\ Fe(III)\text{-reduction}} - \Delta G_{r,\ SO_4\text{-reduction}} > 0$). The AVS and $S^0_{(s)}$ concentrations are shown to illustrate the relationship between the formation of these phases and the relative favourability of Fe(III) versus SO_4-reduction.

mannite and goethite (Fig. 12). Fe(III)-reduction was significantly more favourable than SO_4-reduction throughout the duration of the experiment if Fe(III) was derived from schwertmannite alone (Fig. 12). Accordingly, if schwertmannite remained the phase controlling Fe(III)-supply, then SO_4-reduction would be expected to be negligible for the whole 91-day duration of the column experiment. In contrast, if Fe(III)-supply was instead controlled by goethite solubility, the model calculations predict that Fe(III)-reduction would have dominated over SO_4-reduction only initially (Fig. 12). Following the initial 14–28 day period, the model indicates that reduction of goethite-derived Fe(III) and SO_4 would produce similar energy yields (i.e. $\Delta G_{r,\ Fe(III)\text{-reduction}} - \Delta G_{r,\ SO_4\text{-reduction}}$ remained relatively at $\sim$0 kJ eq^{-1}; Fig. 12). Hence, under these conditions SO_4-reduction products such as AVS and $S^0_{(s)}$ would be predicted to start accumulating at approximately 14–28 days post-inundation depending on depth within the column. The initial observed formation of AVS and $S^0_{(s)}$ contradict the model calculations involving reduction of schwertmannite-derived Fe(III). However, the model calculations based on goethite-derived Fe(III) exhibit reasonable agreement with the observed AVS and $S^0_{(s)}$ data (Fig. 12). This concurs with the XRD and Fe–S extractability data showing substantial goethite formation during the early stages of the column experiment (Figs. 1, 6 and 7).

Overall, the results suggest that the Fe^{II}-catalysed transformation of schwertmannite to goethite acts as a switch inducing a biogeochemical regime shift from a dominance of Fe(III)-reduction to a co-occurrence of simultaneous Fe(III)- and SO_4-reduction. This is consistent with research showing that Fe(III)-reduction in schwertmannite-rich sediment from acidic mine lakes occurs under a range of pH conditions, whereas SO_4-reduction is restricted to near-neutral pH (Blodau, 2006). The partial equilibrium model presented here suggests that this biogeochemical regime shift is directly attributable to the pH-dependency of the Fe^{II}-catalysed transformation of schwertmannite to goethite. Blodau and Peiffer (2003) hypothesize that co-occurrence of Fe(III)- and SO_4-reduction is necessary for Fe(II)-monosulfide accumulation in sediments of acidic mine lakes. This hypothesis is supported by the present results, which demonstrate that significant accumulation of nanoparticulate mackinawite only occurred when reduction of goethite-derived Fe(III) produced similar energy yields to SO_4-reduction (Fig. 12). Accordingly, we propose that Fe^{II}-catalysed transformation of schwertmannite to goethite induces the formation of nanoparticulate mackinawite by facilitating co-occurrence of bacterial Fe(III)- and SO_4-reduction.

4. SUMMARY AND CONCLUSIONS

Drainage of formerly waterlogged, sulfidic soils in coastal lowlands has resulted in severe sulfide-oxidation induced acidification in many areas. Schwertmannite is a major product of this acidification process and its geochemical behaviour is therefore of great importance. Understanding waterlogging-induced transformations of schwertmannite is particularly significant with regard to the re-establishment of wetlands as a potential environmental remediation strategy. The present study provides the first examination of the reductive transformations of Fe and S associated with waterlogging of schwertmannite-rich soil material in acidified coastal lowlands.

Waterlogging of natural schwertmannite- and organic-rich soil material readily induced reduction of schwertmannite-derived Fe(III). This process increased pH to $\sim$6.5, and released Fe^{II}, SO_4 and alkalinity. High concentrations of Fe^{II} and alkalinity allowed precipitation of siderite, which represented the principal sink for Fe^{II}. The present study shows for the first time that interaction

between schwertmannite and Fe^{II} at pH ~6.5 catalyses transformation of schwertmannite to goethite. The extent of this Fe^{II}-catalysed transformation was dependent on pH and the concentrations of Fe^{II} and HCO_3. Model calculations, using a partial equilibrium approach, show that the Fe^{II}-catalysed transformation of schwertmannite to goethite facilitated a biogeochemical regime shift from an initial dominance of Fe(III)-reduction to a co-occurrence of both Fe(III)- and SO_4-reduction. Co-occurrence of Fe(III)- and SO_4-reduction lead firstly to the formation of $S^0_{(s)}$ via H_2S oxidation by goethite and later also to formation of nanoparticulate mackinawite via H_2S precipitation with Fe^{II}. Pyrite formed at rates that were much greater than expected for abiotic systems, yet pyrite was a quantitatively insignificant product of reductive Fe and S mineralisation.

This study demonstrates that reducing conditions, associated with wetland re-establishment in acidified coastal lowlands, is likely to accelerate the transformation of schwertmannite to goethite and cause accumulation of siderite, mackinawite and elemental S. The formation of mackinawite is significant because it leads to improved water quality via consumption of acidity and sequestration of Fe and S. However, the dominance of this highly reactive Fe–S phase over more stable pyrite suggests that such water quality improvements may be rapidly reversed if oxidizing conditions were to recur.

ACKNOWLEDGMENTS

We thank Maxine Dawes for assistance with the SEM–EDX analyses, which were conducted using the SEM Facilities at Southern Cross University. We thank Brian Jones for performing the DOC analyses. The majority of research expenses were funded by the Australian Commonwealth Government through Australian Research Council Grants DP0453280, DP0666334 and DP0772050. The TEM aspects were funded by the Australian Institute of Nuclear Science and Engineering (AINGRA07022). We thank Associate Editor George R. Helz and three anonymous reviewers for very thorough and thoughtful suggestions.

REFERENCES

Acero P., Ayora A., Torrento C. and Nieto H. M. (2006) The behaviour of trace elements during schwertmannite precipitation and subsequent transformation into goethite and jarosite. *Geochim. Cosmochim. Acta* **70**, 4130–4139.

Allison J. P., Brown J. L. and Novo-Gradac K. J. (1991) *MINTEQA2/PRODEFA2, A Geochemical Assessment Model for Environmental Systems*. (Environmental Research Laboratories) United States Environmental Protection Agency. Athens, GA.

Allison J. P. and Purdue E. M. (1994) Modelling metal-humic interactions with MINTEQA2. In *Humic Substances in the Global Environment and Implications on Human Health* (eds. N. Senesi and T. M. Miano). Elsevier Science, Amsterdam.

APHA (1998) *Standard Methods for the Examination of Water and Wastewater*, 20th ed. American Public Health Association—American Water Works Association. Baltimore, USA.

Bartlett J. K. and Skoog D. A. (1954) Colorimetric determination of elemental sulfur in hydrocarbons. *Anal. Chem.* **26**, 1008–1011.

Bigham J. M., Schwertmann U., Carlson L. and Murad E. (1990) A poorly crystallized oxyhydroxysulfate of iron formed by bacterial oxidation of Fe(II) in acid mine waters. *Geochim. Cosmochim. Acta* **54**, 2743–2758.

Bigham J. M., Schwertmann U., Traina S. J., Winland R. L. and Wolf M. (1996a) Schwertmannite and the chemical modeling of iron in acid sulfate waters. *Geochim. Cosmochim. Acta* **60**, 2111–2121.

Bigham J. M., Schwertmann U. and Pfab G. (1996b) Influence of pH on mineral speciation in a bioreactor stimulating acid mine drainage. *Appl. Geochem.* **11**, 845–849.

Bigham J. M. and Nordstrom D. K. (2000) Iron and aluminium hydroxysulfates from acid sulfate waters. In *Sulfate Minerals—Crystallography, Geochemistry and Environmental Significance* (eds. C. N. Alpers, J. L. Jambor and D. K. Nordstrom). Mineral. Soc. Am., Washington, DC. *Rev. Miner. Geochem.* 40, 351–403.

Bigham J. M., Fitzpatrick R. W. and Schulze D. G. (2002) Iron oxides. In *Soil Mineralogy with Environmental Applications* (eds. J. B. Dixon, D. G. Schulze and W. L. Daniels). Soil Science Society of America, Madison, WI.

Blodau C. and Peiffer S. (2003) Thermodynamics and organic matter: constraints on neutralization processes in sediments of highly acidic waters. *Appl. Geochem.* **18**, 25–36.

Blodau C. (2006) A review of acidity generation and consumption in acidic coal mine lakes and their watersheds. *Sci. Total Environ.* **369**, 307–332.

Blodau C. and Gatzek C. (2006) Chemical controls on iron reduction in schwertmannite-rich sediments. *Chem. Geol.* **235**, 366–376.

Blodau C. and Knorr K. H. (2006) Experimental inflow of groundwater induces a "biogeochemical regime shift" in iron-rich and acidic sediments. *J. Geophys. Res.* **111**, G02026.

Burton E. D., Bush R. T. and Sullivan L. A. (2006a) Sedimentary iron geochemistry in acidic waterways associated with coastal lowland acid sulfate soils. *Geochim. Cosmochim. Acta* **70**, 5445–5468.

Burton E. D., Bush R. T. and Sullivan L. A. (2006b) Acid-volatile sulfide oxidation in coastal floodplain drains: iron-sulfur cycling and effects on water quality. *Environ. Sci. Technol.* **40**, 1217–1222.

Burton E. D., Bush R. T. and Sullivan L. A. (2006c) Reduced inorganic sulfur speciation in drain sediments from acid–sulfate soil landscapes. *Environ. Sci. Technol.* **40**, 888–893.

Burton E. D., Bush R. T. and Sullivan L. A. (2006d) Elemental sulfur in drain sediments associated with acid sulfate soils. *Appl. Geochem.* **21**, 1240–1247.

Burton E. D., Bush R. T. and Sullivan L. A. (2006e) Fractionation and extractability of sulfur, iron and trace elements in sulfidic sediments. *Chemosphere* **64**, 1421–1428.

Bush R. T., Fyfe D. and Sullivan L. A. (2004) Occurrence and abundance of monosulfidic black ooze in coastal acid sulfate soil landscapes. *Aust. J. Soil Res.* **42**, 609–616.

Canfield D. E., Thamdrup B. and Fleischer S. (1998) Isotope fractionation and sulfur metabolism by pure and enrichment cultures of elemental sulfur-disproportionating bacteria. *Limnol. Oceanogr.* **43**, 253–264.

Carey E. and Taillefert M. (2005) The role of soluble Fe(III) in the cycling of iron and sulfur in coastal marine sediments. *Limnol. Oceanogr.* **50**, 1129–1141.

Cornell R. M. and Schwertmann U. (2003) *The Iron Oxides: Structure, Properties, Reactions, Occurrences and Uses*. Wiley-VCH.

Dold B. (2003) Dissolution kinetics of schwertmannite and ferrihydrite in oxidized mine samples and their detection by

differential X-ray diffraction (DXRD). *Appl. Geochem.* **18**, 1531–1540.

Donald R. and Southam G. (1999) Low temperature anaerobic bacterial diagenesis of ferrous monosulfide to pyrite. *Geochim. Cosmochim. Acta* **63**, 2019–2023.

Fanning D. S., Rabenhorst M. C., Burch S. N., Islam K. R. and Tangren S. A. (2002) Sulfides and sulfates. In *Soil Mineralogy with Environmental Applications* (eds. J. B. Dixon, D. G. Schulze and W. L. Daniels). Soil Science Society of America, Madison, WI.

Gagliano W. B., Brill M. R., Bigham J. M., Jones F. S. and Traina S. J. (2004) Chemistry and mineralogy of ochreous sediments in a constructed mine drainage wetland. *Geochim. Cosmochim. Acta* **68**, 2119–2128.

Gieskes J. M. and Rogers C. W. (1973) Alkalinity determination in interstitial waters of marine sediments. *J. Sediment. Petrol.* **43**, 272–277.

Hansel C. M., Benner S. G. and Fendorf S. (2005) Competing Fe(II)-induced mineralization pathways of ferrihydrite. *Environ. Sci. Technol.* **39**, 7147–7153.

Hsieh Y. P., Chung S. W., Tsau Y. J. and Sue C. T. (2002) Analysis of sulfides in the presence of ferric minerals by diffusion methods. *Chem. Geol.* **182**, 195–201.

Jensen D. L., Boddum J. K., Tjell J. C. and Christensen T. H. (2002) The solubility of rhodochrosite ($MnCO_3$) and siderite ($FeCO_3$) in anaerobic aquatic environments. *Appl. Geochem.* **17**, 503–511.

Jonsson J., Persson P., Sjoberg S. and Lovgren L. (2005) Schwertmannite precipitated from acid mine drainage: phase transformation, sulphate release and surface properties. *Appl. Geochem.* **20**, 179–191.

Knorr K. H. and Blodau C. (2006) Experimentally altered groundwater inflow remobilizes acidity from sediments of an iron rich and acidic lake. *Environ. Sci. Technol.* **40**, 2944–2950.

Kostka J. E. and Luther G. W. (1994) Partitioning and speciation of solid phase iron in saltmarsh sediments. *Geochim. Cosmochim. Acta* **58**, 1701–1710.

Kumpulainen S., Carlson L. and Raisanen M-L. (2007) Seasonal variations of ochreous precipitates in mine effluents in Finland. *Appl. Geochem.* **22**, 760–777.

Langmuir D. (1997) *Aqueous Environmental Geochemistry*. Prentice-Hall Publishers, New Jersey, USA.

Majzlan J., Navrotsky A. and Schwertmann U. (2004) Thermodynamics of iron oxides: part III. Enthalpies of formation and stability of ferrihydrite ($\sim Fe(OH)_3$), schwertmannite ($\sim FeO(OH)_{3/4}(SO_4)_{1/8}$), and ε-Fe_2O_3. *Geochim. Cosmochim. Acta* **68**, 1049–1059.

Murad E. and Rojik P. (2003) Iron-rich precipitates in a mine drainage environment: influence of pH on mineralogy. *Am. Mineral.* **88**, 1915–1918.

Ohfuji H. and Rickard D. (2006) High resolution transmission electron microscopic study of synthetic nanocrystalline mackinawite. *Earth Planet. Sci. Lett.* **241**, 227–233.

Parker V. B. and Khoakovskii I. L. (1995) Thermodynamic properties of the aqueous ions (2+ and 3+) of iron and the key compounds of iron. *J. Phys. Chem. Ref. Data* **24**, 1699–1745.

Pedersen H. D., Postma D., Jakobsen R. and Larsen O. (2005) Fast transformation of iron oxyhydroxides by the catalytic action of aqueous Fe(II). *Geochim. Cosmochim. Acta* **69**, 3967–3977.

Peine A., Tritschler A., Kusel K. and Peiffer S. (2000) Electron flow in an iron-rich acidic sediment—evidence for an acidity-driven iron cycle. *Limnol. Oceanogr.* **45**, 1077–1087.

Phillips E. J. P. and Lovley D. R. (1987) Determination of Fe(III) and Fe(II) in oxalate extracts of sediments. *Soil Sci. Soc. Am. J.* **51**, 938–941.

Postma D. and Jakonsen R. (1996) Redox zonation: Equilibrium constraints on the Fe(III)/SO_4-reduction interface. *Geochim. Cosmochim. Acta* **60**, 3169–3175.

Rayment G. E. and Higginson F. R. (1992) *Australian Laboratory Handbook of Soil and Water Chemical Methods*. Inkata Press, Melbourne.

Regenspurg S., Brand A. and Peiffer S. (2004) Formation and stability of schwertmannite in acidic mining lakes. *Geochim. Cosmochim. Acta* **68**, 1185–1197.

Regenspurg S. and Peiffer S. (2005) Arsenate and chromate incorporation in schwertmannite. *Appl. Geochem.* **20**, 1226–1239.

Rickard D. (1974) Kinetics and mechanism of the sulfidization of goethite. *Am. J. Sci.* **274**, 941–952.

Rickard D. T. (1995) Kinetics of FeS precipitation, part 1: competing reaction mechanisms. *Geochim. Cosmochim. Acta* **59**, 4367–4379.

Rickard D. and Morse J. W. (2005) Acid volatile sulfide (AVS). *Mar. Chem.* **97**, 141–197.

Rickard D. (2006) The solubility of FeS. *Geochim. Cosmochim. Acta* **70**, 5779–5789.

Rickard D., Griffith A., Oldroyd A., Butler I. B., Lopez-Capel E., Manning D. A. C. and Apperley D. C. (2006) The composition of nanoparticulate mackinawite, tetragonal iron(II) monosulfide. *Chem. Geol.* **235**, 286–298.

Roden E. E. and Urrutia M. M. (1999) Ferrous iron removal promotes microbial reduction of crystalline iron (III) oxides. *Environ. Sci. Technol.* **33**, 1847–1853.

Schippers A. and Jorgensen B. B. (2001) Oxidation of pyrite and iron sulfide by manganese dioxide in marine sediment. *Geochim. Cosmochim. Acta* **65**, 915–922.

Steudel R. and Eckert B. (2004) Solid sulfur allotropes. In *Elemental Sulfur and Sulfur-rich Compounds II (Topics in current chemistry)* (ed. R. Steudel). Springer, New York.

Stumm W. and Morgan J. J. (1996) *Aquatic Chemistry*, third ed. Wiley, New York.

Sullivan L. A. and Bush R. T. (1997) Quantitative microanalysis of rough soil surfaces in the scanning electron microscope using a peak-to-background method. *Soil Sci.* **162**, 749–757.

Sullivan L. A., Bush R. T. and McConchie D. M. (2000) A modified chromium-reducible sulfur method for reduced inorganic sulfur: optimum reaction time for acid sulfate soil. *Aust. J. Soil Res.* **38**, 729–734.

Sullivan L. A., Bush R. T. and Fyfe D. (2002) Acid sulfate soil drain ooze: distribution, behaviour and implications for acidification and deoxygenation of waterways. In *Acid Sulfate Soils in Australia and China* (eds. C. Lin, M. D. Melville and L. A. Sullivan). Science Press, Beijing, pp. 91–99.

Sullivan L. A. and Bush R. T. (2004) Iron precipitate accumulations associated with waterways in drained coastal acid sulfate landscapes of eastern Australia. *Mar. Freshwater Res.* **55**, 727–736.

Sullivan L. A., Cabot Y., Bush R. T. and Burton E. D. (2006) Schwertmannite in acid sulfate subsoils and associated groundwater geochemistry. *Geochim. Cosmochim. Acta* **70**(Suppl. 1), A624.

Tulau M. J. (2002) Agricultural drainage in acid sulfate soil backswamps in New South Wales, Australia—technical, regulatory and policy responses. In *Acid Sulfate Soils in Australia and China* (eds. C. Lin, M. D. Melville and L. A. Sullivan). Science Press, Beijing, China.

Wagman D. D., Evans W. H., Parker V. B., Halow I., Bailey S. M. and Schumm, R. H. (1968) *Selected Values of Chemical Thermodynamic Properties: Tables for the First Thirty-four Elements in the Standard Order*, pp. 270–273. National Bureau of Standards (US), Technical Note.

Webster J. G., Swedlund P. J. and Webster K. S. (1998) Trace metal adsorption onto an acid mine drainage iron(III) oxy-hydroxysulfate. *Environ. Sci. Technol.* **32**, 1361–1368.

Wolthers M., Van der Gaast S. J. and Rickard D. (2003) The structure of disordered mackinawite. *Am. Mineral.* **88**, 2007–2015.

Yao W. and Millero F. J. (1996) Oxidation of hydrogen sulfide by hydrous Fe(III) oxides in seawater. *Mar. Chem.* **52**, 1–16.

Yu J. Y., Heo B., Choi I., Cho J. and Chang H. (1999) Apparent solubilities of schwertmannite and ferrihydrite in natural stream waters polluted by mine drainage. *Geochim. Cosmochim. Acta* **63**, 3407–3416.

Associate editor: George R. Helz